Driveline oscillation attenuation through Clutch Micro-Slip and Model Predictive Control

Control Engineering Practice 140 (2023) 105672

Contents lists available at ScienceDirect

Control Engineering Practice

journal homepage: www.elsevier.com/locate/conengprac

Driveline oscillation attenuation through Clutch Micro-Slip and Model Predictive Control

Massimo Canale [a,*], Vito Cerone [a], Emanuel Corigliano [b], Giancarlo Osella [b]

[a] Dipartimento di Automatica e Informatica, Politecnico di Torino, Italy
[b] Centro Ricerche Fiat, Italy

ARTICLE INFO

Keywords:
Driveline oscillations
Transmission systems
Model predictive control

ABSTRACT

This paper considers a Model Predictive Control (MPC) approach to micro-slip clutch control for driveline shuffle attenuation and longitudinal acceleration oscillation reduction in vehicles with an Automated Manual Transmission system. We introduce an original MPC formulation to consider the performance tradeoff between the clutch slip regulation, the torsional oscillation attenuation and the jerking reduction. A particular problem to be considered is handling saturation constraints on the transmitted torque. We employ a piecewise-affine linear model of the actuator-driveline system to take care of special manoeuvres that cause inversions in the transmission motion. On the methodological side, we present a switching MPC approach where the underlying optimization problem is a quadratic programme for a fast online controller implementation on real-world transmission control unit platforms. To show the effectiveness of the proposed approach, we present extensive simulation results and experimental tests performed on a prototype vehicle.

1. Introduction

The automotive industry invests considerable resources to improve driving comfort and fuel efficiency for the commercial success of vehicles through the development of advanced transmission and powertrain systems. Standard manual transmission (MT) systems lead to uneven gear shift operation and torque transmission disruption, which may worsen the comfort and gas consumption performance. Automated manual transmission (AMT) systems provide significant enhancements (see, e.g. Fischer et al. (2015)) over MT systems, thanks to direct handling of clutch actuation and gear shift actions through hydraulic actuators driven by a suitable control algorithm.

In particular, the gear shift is more smooth and with limited traction interruptions in AMT systems with the dual-clutch transmission (DCT) technology (see Fischer et al. (2015)), the gear shift can be achieved more smoothly and with limited traction interruptions. However, torsional oscillations may occur across the transmission driveline during, e.g., tip-in and tip-out manoeuvres because of the elastic characteristics of the mechanical components. Such fluctuations are also referred to as "shuffles" (see e.g. Kiencke and Nielsen (2005)), and generate longitudinal jerking effects that, in turn, cause a loss of vehicle driveability and comfort. In the past years, designers have devised several control methods and architectures to weaken the effects of driveline shuffles. The main approaches rely on different strategies such as the control of (a) the engine air/fuel ratio (see e.g. Pettersson and Nielsen (2003)), (b) the engine spark advance (see e.g. Berriri et al. (2008)) and (c) the electronic gas pedal (see e.g. Northcote (2006)). In this context, Lefebvre et al. (2003) propose a robust control approach based on H_∞ optimization, Berriri et al. (2008) employ a robust pole placement methodology, while Naus et al. (2008) consider a μ-synthesis technique. Robust control methodologies using both H_∞ and μ-synthesis techniques are employed in Buerger and Anderson (2019) for shuffle attenuation in electric powertrains using a two-degrees of-freedom architecture and in Corno et al. (2021) by considering a data-driven approach to control the driveline oscillations through black-box identification of the main oscillation modes and active damping control. In Ravichandran et al. (2020), the authors design and evaluate a torque-shaping switching control system to mitigate the clunk, i.e., the oscillation effect induced by the gearbox backlash, and the shuffle of an electric vehicle drivetrain.

In the field of optimal control, Bruce et al. (2005) employ LQR methods to design a combined feedback and feedforward controller, while Fredriksson et al. (2002) and Templin and Egardt (2009) present LQG/LTR methodologies. Lagerberg and Egardt (2005) and Rostalski

* Corresponding author.
E-mail address: massimo.canale@polito.it (M. Canale).

https://doi.org/10.1016/j.conengprac.2023.105672
Received 26 November 2022; Received in revised form 18 August 2023; Accepted 19 August 2023
Available online 6 September 2023

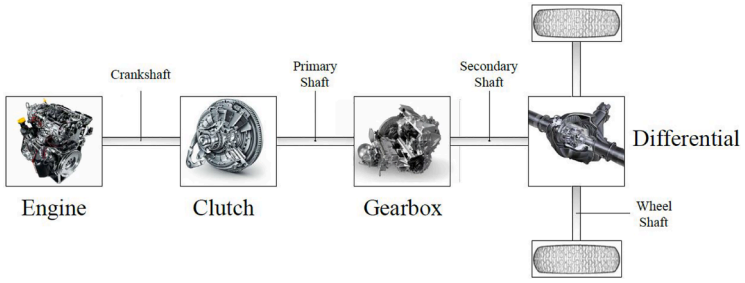

Fig. 1. Driveline scheme.

et al. (2007) proposed Model Predictive Control (MPC) strategies to limit the clunk phenomenon. More recently, in the same context, Reddy et al. (2023) have designed and implemented a drivetrain torque shaping controller using a soft landing reference governor approach combined with the one-step ahead prediction of the backlash position. Baumann et al. (2006) and Caruntu et al. (2016) exploit anti-jerk MPC controllers that prevent the driveline from oscillating. However, as Mashadi and Badrykoohi (2015) highlighted, the engine torque control methods outlined above may carry some disadvantages. For example, in the engine control method through spark advance, altering the spark timing against the original combustion settings may, in general, impair engine pollution. Moreover, in both the air/fuel ratio and electronic gas pedal control methods, changes in the driver torque demand lead to a reduction in vehicle performance and unacceptable behaviours for many drivers. Albers (1990) introduced an effective solution to overcome such disadvantages by forcing a suitable clutch slip action using the modulation of the clutch transmitted torque. However, the energy dissipated in the clutch disks during the slipping gives rise to wear and overheating effects. Therefore, to avoid system failures, the slipping speed between the engine and the primary shaft of the transmission line must be maintained as low as possible. For this reason, such oscillation reduction strategy is known as clutch "micro-slip" control. Fischer and Berger (1998) and in Audi of America Inc. (2001) describe applications of micro-slip control on commercial vehicles. The literature reports different approaches for micro-slip control of transmission systems. Mashadi and Badrykoohi (2015) and Hebbale et al. (2011), and Lee (2015) proposed basic feedback and feedforward schemes, respectively. Myklebust (2014) considers an LQR controller combined with an extended Kalman estimator, while Higashimata et al. (2004) designed a robust controller through μ-synthesis techniques. Gao et al. (2011) employ backstepping methods, whereas Kaneko et al. (2009) adopt gain scheduling techniques. Micro-slip control is also employed in Wang and Lu (2022) to reduce oscillations during gearshift manoeuvres in a DCT system using MPC methodologies.

In this work, we present an original solution to the clutch micro-slip control through MPC methodologies inspired by Canale et al. (2017) that introduce preliminary results of this study in a simplified context. The first reason for choosing MPC techniques is that they appear to be relatively successful in the control of advanced AMT and DCT transmission systems, as reported by Bemporad et al. (2001), Lagerberg and Egardt (2005), Baumann et al. (2006), Rostalski et al. (2007), Caruntu et al. (2013), Pisaturo et al. (2015), Lu et al. (2015), Caruntu et al. (2016) and Wang and Lu (2022). Secondly, MPC is an attractive approach for systems with fast dynamics, thanks to recent technological advances. Furthermore, MPC design can handle conflicting multi-objective control problems and consider constraints on both the command inputs and the controlled outputs, allowing the system to work closer to its physical limitations and improve overall performance.

In this paper, we exploit the MPC features for a practical problem formulation of clutch micro-slip control of AMT systems. We show how to manage the performance compromise between the slipping speed reference tracking and the torsional oscillation attenuation using the definition of a suitable quadratic cost index. We consider saturation

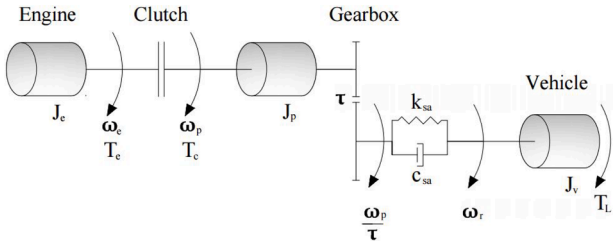

Fig. 2. Driveline simplified model.

constraints on the transmitted clutch torque input and explicitly account for clutch actuator dynamics and delay in the controller design. Our approach uses a more general setting for the driveline dynamics. The proposed method accounts for situations when the transmission system is subject to sudden acceleration changes, as in tip-out manoeuvres in the presence of an abrupt gas pedal release that causes a fall of the engine torque and a sign inversion of the driveline motion. We employ a linear piecewise-affine (PWA) model of the driveline to describe all the considered working situations. Such a modelling approach allows us to exploit a switching MPC method based on quadratic programming (QP) in the underlying optimization problem. This formulation, thanks to the available QP solvers (see e.g. Ferreau et al. (2008)), leads to fast online execution of the MPC control law on regular transmission control unit (TCU) platforms.

The organization of the paper is as follows. Section 2 introduces the modelling of the considered driveline and the actuator systems. In Section 3, we formulate the problem of micro-slip control in the MPC framework. In Sections 4 and 5, we perform extensive simulation tests and report the obtained experimental results on a real prototype vehicle to show the effectiveness of the proposed approach. Section 6 ends the paper with concluding remarks.

2. Driveline and actuator modeling for micro-slip control

2.1. Driveline model

The vehicle driveline system transfers the engine torque to the driving wheels (see Fig. 1) through the fundamental parts that can be summarized as: crankshaft, clutch, main shaft, gearbox, secondary shaft, differential and wheel shaft.

Linear driveline models with different levels of complexity in terms of the number of degrees of freedom (d.o.f.) play a crucial role in the control design of vehicle transmission systems. On the other hand, as noted in Pisaturo et al. (2015), using simple models, i.e. with a small number of d.o.f., may improve the computational effort needed for the MPC controller online implementation. Along the same line, in this work, we consider the simplified three masses linear model with a flexible secondary shaft, introduced in Dolcini et al. (2005) and represented in Fig. 2, to describe the driveline dynamics during the slipping of the clutch. Such a model does not consider the nonlinear characteristics of the transmission line, such as the gear backlash and the tyre slip, and

Table 1
Driveline Model Parameter Description.

Parameter	Symbol
Engine inertia	J_e
Engine damping coefficient	c_e
Main shaft inertia	J_p
Gear ratio	τ
Secondary shaft damping coefficient	c_{sa}
Secondary shaft stiffness	k_{sa}
Vehicle mass	M
Wheel radius	r_w
Wheel inertia	J_w
Vehicle inertia	$J_v = Mr_w^2 + J_w$

retains that the engine acts as a mean value torque generator, not including the high-frequency dynamic behaviour. The final assumptions are that the main shaft is rigid and the driveshafts are symmetric.

Table 1 describes the physical parameters of the driveline.

In the model represented in Fig. 2, ω_e is angular speed of the engine shaft, ω_p represents the angular speed of the primary shaft and ω_r stands for the angular speed of the drive shaft. The corresponding angular positions are indicated as ϑ_e, ϑ_p and ϑ_r, respectively. The model inputs are the engine torque T_e, the clutch torque T_c and the load torque T_L. More precisely, the clutch torque is supposed to be the only manipulable input while the engine torque and the load torque are assumed as measurable disturbances.

The clutch torque T_c drives the slipping of the clutch plates with respect to the engine flywheel. During the slipping phase, the clutch torque T_c switches its sign according on the one of the slipping speed $\omega_d = \omega_e - \omega_p$ as described in (1), see, e.g., Lhomme et al. (2008) for details.

$$T_c = \begin{cases} T_c \text{ if } \omega_d \geq 0 \\ -T_c \text{ if } \omega_d < 0 \end{cases} \tag{1}$$

This occurence typically arises in the presence of sudden acceleration changes as happens, e.g., in tip-out maneuvers when an abrupt gas pedal release causes a fall of the engine torque and a sign inversion of the driveline motion described by ω_d.

The load torque T_L includes the effects of the aerodynamic resistance force F_a, the rolling resistance force F_r, the road slope driving force F_g and the braking force F_b as described by equation (2).

$$T_L = \left(F_a + F_r + F_g + F_b\right) r_w \tag{2}$$

The forces F_a, F_r and F_g are given by:

$$\begin{aligned} F_a &= 0.5\rho_a A_f \beta_a (v_v - v_w)^2 \\ F_r &= Mg\mu_r \cos(\alpha) \\ F_g &= Mg\sin(\alpha) \end{aligned}$$

where:

- A_f is the vehicle frontal area,
- β_a is the aerodynamic drag coefficient,
- v_v is the vehicle speed,
- v_w is the wind speed,
- ρ_a is the air density,
- μ_r is the rolling friction coefficient,
- α is the road slope angle,
- g is the gravity acceleration.

Finally, we assume that the only measured variables are ω_e, ω_p and ω_r.

According to the scheme reported in Fig. 2, and introducing the torsion angular position ϑ_{sr} and speed ω_{sr} as:

$$\begin{aligned} \vartheta_{sr}(t) &= \frac{\vartheta_p(t)}{\tau} - \vartheta_r(t) \\ \omega_{sr}(t) &= \dot{\vartheta}_{sr}(t) \end{aligned} \tag{3}$$

the driveline dynamics are described by the follwing set of differential equations:

$$\begin{aligned} J_e\dot{\omega}_e(t) &= -c_e\omega_e + T_e(t) - \text{sign}(\omega_d(t))\, T_c(t) \\ J_p\dot{\omega}_p(t) &= -\frac{c_{sa}}{\tau^2}\omega_p(t) + \frac{c_{sa}}{\tau}\omega_r(t) - \frac{k_{sa}}{\tau}\vartheta_{sr}(t) + \text{sign}(\omega_d(t))T_c(t) \\ J_v\dot{\omega}_r(t) &= \frac{c_{sa}}{\tau}\omega_p(t) - c_{sa}\omega_r(t) + k_{sa}\vartheta_{sr}(t) + T_L(t) \\ \dot{\vartheta}_{sr}(t) &= \frac{\omega_p(t)}{\tau} - \omega_r(t) \end{aligned} \tag{4}$$

The clutch torque T_c is realized through an electro-hydraulic actuator that is controlled by regulating the clutch throw-out bearing position to a reference value that is determined through a static map based on the clutch torque request T_c^{req}, see, for details Canale et al. (2017). This study considers the actuator and its control as a lumped dynamical system with input T_c^{req} and output T_c that can be approximated by a 2nd order transfer function of the form:

$$G_{act}(s) = \frac{T_c(s)}{T_c^{\text{req}}(s)} = K_t \frac{\omega_n^2}{s^2 + 2\zeta\omega_n s + \omega_n^2} e^{-\theta s} \tag{5}$$

In (5), $K_t = 1$ is the clutch transmissibility gain, $\theta = 10$ ms is the overall actuation delay, while $\zeta = 0.81$ and $\omega_n = 55$ rad/s are the pole damping coefficient and natural frequency respectively. Note that, in the simplified model (5), variations on the clutch transmissibility characteristics due to, e.g., the temperature at different operating conditions, wear and ageing, can be approximately described by a parametric uncertainty on the coefficient K_t, see Canale et al. (2017) for details.

2.2. Complete actuator-driveline model for MPC micro-Slip control design

For MPC micro-slip control design, we need a state space model of the combined actuator-driveline connection.

Introducing the driveline state vector x_d as:

$$x_d(t) = \left[\omega_e(t), \omega_p(t), \omega_r(t), \vartheta_{sr}(t)\right]^T \in \mathbb{R}^4 \tag{6}$$

the driveline dynamic equation (4) together with the switching mode (1) can be expressed in the state space form as:

$$\dot{x}_d(t) = A^d x_d(t) + B^{d,e} T_e(t) + B^{d,L} T_L(t) + \gamma(t) B^{d,c} T_c(t) \tag{7}$$

where A^d, $B^{d,e}$, $B^{d,L}$ and $B^{d,c}$ are the following matrices

$$A^d = \begin{bmatrix} -\frac{c_e}{J_e} & 0 & 0 & 0 \\ 0 & -\frac{c_{sa}}{J_p\tau^2} & \frac{c_{sa}}{J_p\tau} & -\frac{k_{sa}}{J_p\tau} \\ 0 & \frac{c_{sa}}{J_v\tau} & -\frac{c_{sa}}{J_v} & \frac{k_{sa}}{J_v} \\ 0 & \frac{1}{\tau} & -1 & 0 \end{bmatrix}, B^{d,e} = \begin{bmatrix} \frac{1}{J_e} \\ 0 \\ 0 \\ 0 \end{bmatrix}, B^{d,L} = \begin{bmatrix} 0 \\ 0 \\ \frac{1}{J_v} \\ 0 \end{bmatrix}, B^{d,c} = \begin{bmatrix} -\frac{\gamma(t)}{J_e} \\ \frac{\gamma(t)}{J_p} \\ 0 \\ 0 \end{bmatrix} \tag{8}$$

In (8), the factor $\gamma(t)$ accounts for (1) and is given by:

$$\gamma(t) = \begin{cases} 1 \text{ if } \omega_d(t) \geq 0 \\ -1 \text{ if } \omega_d(t) < 0 \end{cases} \tag{9}$$

As to the controlled actuator system described by (5), a 2nd order state space description can be obtained by means of the control canonical form realization as:

$$\begin{aligned} \dot{x}_a(t) &= A^a x_a(t) + B^a T_c^{\text{req}}(t - \theta) \\ T_c(t) &= C^a x_a(t) \end{aligned} \tag{10}$$

where $x_a \in \mathbb{R}^2$ is the actuator state vector. Notice that, given the instrumental function of the control canonical form, we can not attribute a physical meaning to the state x_a. The matrices A_a, B_a and C_a in (10) are

$$A^a = \begin{bmatrix} 0 & 1 \\ -\omega_n^2 & -2\zeta\omega_n \end{bmatrix} \quad B^a = \begin{bmatrix} 0 \\ 1 \end{bmatrix}$$
$$C^a = \begin{bmatrix} K_t\omega_n^2 & 0 \end{bmatrix} \tag{11}$$

Since the design of the MPC controller requires a discrete time model, the state representations (7) and (10) have been discretized with sampling time $T_s = \theta$ using the backward Euler method. The delayed input $T_c^{\text{req}}(t-\theta)$ is described by the additional discrete time state variable x_θ defined as

$$x_\theta(k) = T_c^{\text{req}}(k-1) \tag{12}$$

The resulting discrete time state equations of the driveline and the actuator are:

$$x_d(k+1) = \overline{A}^d x_d(k) + \overline{B}^{d,e} T_e(k) + \overline{B}_d^L T_L(k) + \gamma(k)\overline{B}^{d,c} T_c(k) \tag{13}$$

$$\begin{aligned} x_a(k+1) &= \overline{A}^a x_a(k) + \overline{B}^a x_\theta(k) \\ x_\theta(k+1) &= T_c^{\text{req}}(k) \\ T_c(k) &= \overline{C}^a x_a(k) \end{aligned} \tag{14}$$

To simplify the notation, in (12), (13) and (14), the time variable k is used to denote the integer multiple of the sampling time T_s, i.e. $k = \ell T_s$, $k, \ell \in \mathbb{N}$.

Introducing the overall state variable x defined as

$$x = [x_d, x_a, x_\theta]^T \in \mathbb{R}^7, \tag{15}$$

the complete state equation of the Actuator-Driveline system are given by

$$x(k+1) = A_\gamma x(k) + B T_c^{\text{req}}(k) + B^e T_e(k) + B^L T_L(k) \tag{16}$$

where

$$A_\gamma = \begin{bmatrix} \overline{A}^d & \gamma(k)\overline{B}^{d,c}\overline{C}^a & 0_{4,1} \\ 0_{2,4} & \overline{A}^a & \overline{B}^a \\ 0_{1,4} & 0_{1,2} & 0 \end{bmatrix} \quad B = \begin{bmatrix} 0_{4,1} \\ 0_{2,1} \\ 1 \end{bmatrix} \quad B^e = \begin{bmatrix} \overline{B}^{d,e} \\ 0_{2,1} \\ 0 \end{bmatrix} \quad B^L = \begin{bmatrix} \overline{B}^{d,L} \\ 0_{2,1} \\ 0 \end{bmatrix} \tag{17}$$

and

$$\gamma(k) = \begin{cases} 1 \text{ if } \omega_d(k) \geq 0 \\ -1 \text{ if } \omega_d(k) < 0 \end{cases} \tag{18}$$

In (17), the notation $0_{i,j}$ represents an $i \times j$ matrix of zeros.

Because of the presence of the switching parameter γ in the dynamic matrix A_γ in (17), the Actuator-Driveline model introduced in (16) represents a Piecewise Affine (PWA) System, see e.g. Borrelli et al. (2017), with two switching modes.

3. Micro-slip control using MPC

3.1. Problem formulation

As described in Section 1, the micro-slip control aims at imposing a suitable clutch slip action to attenuate the driveline torsional oscillations. In the controller design, such a slip action can be realized by making the clutch slipping speed $\omega_d = \omega_e - \omega_p$ track a suitable reference signal ω_d^{ref}.

On the other hand, as considered in Caruntu et al. (2016), the driveline oscillation attenuation can be accounted for through the zero regulation of the torsion speed ω_{sr} defined in (3). Thus, the design requirements for clutch micro-slip control can be summarized as:

R$_1$ Reference tracking of the clutch slipping speed ω_d by minimization of the tracking error e_d defined as:

$$e_d = \omega_d^{\text{ref}} - \omega_d. \tag{19}$$

R$_2$ Zero regulation of the torsion speed ω_{sr}.

The micro-slip control design procedure has to be suitably carried out in order to achieve an "optimal" tradeoff between requirements R$_1$ and R$_2$.

The controller design is performed using the PWA model described by (16). Furthermore, since the only measured variables are ω_e, ω_p and ω_r, we need a suitable state observer to obtain an estimate of the state values at each sampling time.

As observed in Section 2, the slip control action is obtained by modulating the clutch torque input whose values are subject to the physical limitations of the actuator device. As a consequence, a saturation constraint on the clutch torque T_c has to be included in the controller design procedure to account for such limitations. Although the transmitted clutch torque T_c is not measurable, thanks to the use of the state observer we obtain an estimate $\widehat{T}_c$ through (14). Thus, a constraint of the form (20) is imposed in the design procedure.

$$0 < \widehat{T}^c(k) \leq \overline{T}_c, \forall k \in \mathbb{N} \tag{20}$$

The MPC approach for the micro-slip controller design in the presence of constraints and a PWA model of the plant is well motivated in the literature, as already noted in Section 1. Caruntu et al. (2016) used a PWA driveline model to account for the piecewise-linear characteristic of the clutch stiffness, while Di Cairano et al. (2010) described the relationship between the wheel side-slip angle and the tyre force as piecewise-linear function leading to a PWA model of the vehicle lateral dynamics.

3.2. MPC Formulation of micro-slip clutch control

According to the introduced design settings, the micro-slip MPC design in terms of the following finite horizon optimization problem, which must be solved at each sampling time:

$$\min_{\mathscr{T}_c(k)} J(k)$$

$$J(k) = \sum_{i=0}^{N-1} q_d e_d^2(k+i+1|k) + q_{sr}\omega_{sr}^2(k+i+1|k) +$$

$$+ r_c T_c^{\text{req}\,2}(k+i|k) + q_\varepsilon \varepsilon^2$$

$$\mathscr{T}_c(k) = \left[T_c^{\text{req}}(k|k), \cdots, T_c^{\text{req}}(k+N-1|k), \varepsilon\right] \tag{21}$$

s.t.

equations (16), (17), (18)

$$0 < \widehat{T}_c(k+i|k) \leq \overline{T}_c + \varepsilon, i = 0, \ldots, N-1$$

$$e_d(k+N|k) = 0$$

In (21), N is the prediction horizon while the terms $e_d(k+i|k))$ and

$\omega_{sr}(k+i|k)$ represent, respectively, the i[th] step ahead prediction of the tracking error based on the estimated slipping speed and the estimated torsional speed computed using model (16).

The weight coefficients $q_d \in \mathbb{R}^+$, $q_{sr} \in \mathbb{R}^+$, $r_c \in \mathbb{R}^+$ and $q_\varepsilon \in \mathbb{R}^+$ in (21) are design tuning parameters to achieve a suitable tradeoff among requirements R_1 and R_2 and the requested clutch torque T_c^{req} effort. Moreover, to account for the contributions of the measurable inputs T_e and T_L, we assume that both T_e and T_L are kept constant at the value actually measured at the current sampling instant k, i.e. $T_e(k+i|k) = T_e(k), T_L(k+i|k) = T_L(k), i = 0,\dots,N$, within the prediction horizon N. The terminal tracking error constraint $e_d(k+N|k) = 0$ in (21) is added to guarantee nominal asymptotic stability of the controlled system, as described, e.g., in Grüne and Pannek (2011). The last term of the cost function J in (21), i.e. $q_\varepsilon \varepsilon^2$, accounts for the slack variable ε introduced to handle the soft constraints on the estimated transmitted clutch torque $\widehat{T}_c$ to prevent its infeasibility.

The minimizer of (21) at sampling time k is denoted by:

$$\begin{aligned} \mathscr{T}_c^O(k) &= \underset{\mathscr{T}_c}{\text{argmin}} J(k) = \\ &= \left[T_c^{\text{req}\,O}(k|k), \cdots, T_c^{\text{req}\,O}(k+N-1|k) \cdots, \varepsilon^O\right] \end{aligned} \tag{22}$$

then, according to the receding horizon principle (see e.g. Mayne and Rawlings (2012)) the actual clutch torque control move is obtained as the first component of $\mathscr{T}_c^O(k)$ as:

$$T_c^{\text{req}}(k) = T_c^{\text{req}\,O}(k|k) \tag{23}$$

The minimization problem in (21) can be casted in the framework of mixed integer quadratic programming (MIQP) optimization, see Borrelli et al. (2017). However, the solution of such a problem requires a significant computational burden that prevents the practical online implementation of the MPC micro-slip controller on a commercial transmission control unit (TCU). However, in the PWA model described by (16)-(18), there are only two switching modes that do not depend on the system input. For this reason, the simpler switching MPC approach introduced in Di Cairano et al. (2010), can be successfully employed. Such a switching approach assumes that during the prediction horizon there are not mode switches. In this way, at every sampling time k, we obtain the value $\gamma(k)$ through (18) and set the corresponding state matrix A_γ. At this point, the model (16) becomes a linear time invariant (LTI) system and the optimization problem (21) comes to be a quadratic program (QP). As a result, thanks to the recently developed efficient QP solvers that employ advanced active set methods (see e.g. Ferreau et al. (2008)), we can derive a fast online implementation of the MPC controller on available commercial TCU platforms. With such settings the state observer is designed using standard approaches for LTI systems for each of the switched model. For example, a Luenberger observer can be used for both the models described by (16)-(17). The case of more general linear observers as in Canale et al. (2008) can be handled in a similar way.

Note that, because of the presence of the state observer, we should adopt a suitable robust MPC design method that explicitly takes into account the state estimation error. In this regard, a possible solution is to make tighter, i.e., more restrictive the constraints introduced in (21) to account for the estimation error, as described in Mayne et al. (2006). However, such an approach may lead to a more conservative design procedure and, in turn, to optimization problem infeasibility and to performance degradation. For this reason, we perform the MPC design without considering the effects of the state estimation errors and exploiting the robustness properties inherited by the nominal formulation of the optimization problem (21). As to the inherent stability properties of MPC, Heath and Wills (2005) introduce sufficient conditions based on the input weight of the cost function in the case of asymptotically stable plants. The inherent stability principle of MPC is employed in Pisaturo et al. (2015) for the engagement control of a dry clutch.

Table 2
Control Design Parameter.

Parameter	N	q_d	q_{sr}	r_c	q_ε
Value	5	380	120	20	1

4. Simulation results

In this Section we introduce simulation results aimed at showing the effectiveness of the proposed approach. We have performed such tests using a 5 degrees of freedom Simulink transmission model, which includes nonlinear characteristics such as gear backlash and tyre slip and gives a quite accurate description of the driveline dynamics as compared to actual measurements (see Lancia (2014)). We have considered model (5) to describe the controlled actuator device. We have carried out the MPC design through optimization problem (21) with sampling time $T_s =$ 10 ms. The desired steady state reference slipping speed ω_d^{ref} is a constant value of 50 rpm, when $\gamma(k) = 1$ and -50 rpm, when $\gamma(k) = -1$. As to constraint (20), we have set $\overline{T}_c = 250$ Nm. A trial and error procedure has been followed to tune the design parameters N, q_d, q_{sr}, r_c q_{sr} and q_ε until a satisfactory performance tradeoff is achieved. In Table 2 the resulting parameter values are reported.

We have designed a standard Luenberger observer to obtain the state estimate for both the considered switched models. As a realistic simulation scenario, a sequence of sudden acceleration and deceleration manoeuvres performed on a flat road, i.e. $\alpha = 0 \rightarrow F_g = 0$, has been considered to test the micro-slip effects when the 3[rd] gear is engaged. First, we have performed a simulation test when the transmissibility coefficient K_t in (5) is set to its nominal value. The considered manoeuvre is realized by imposing the engine torque input reported in green in the top plot of Fig. 3 and without braking force, i.e. $F_b = 0$.

Notice that the course of the engine torque at about 7 s ranges from the positive value of 200 Nm to the negative value of -20 Nm. Such a profile corresponds to a sudden release of the accelerator pedal, i.e. a tip-out manoeuvre, that causes the sign inversion of the angular speed ω_d and consequently the switch of the mode γ.

In Fig. 3, the achieved performance is reported in terms of clutch torque and slipping speed tracking. In particular, in the top plot of Fig. 3 the requested clutch torque T_c^{req} (blue) is reported together with the actually transmitted torque T_c (black) and its estimate $\widehat{T}_c$ (red). Notice that, except for a slight delay, in the absence of transmissibility perturbation, the transmitted torque T_c coincides with the requested one T_c^{req}. In the bottom plot of Fig. 3, the slipping speed ω_d (blue line) is reported and compared with the reference signal ω_d^{ref} (red line).

The two pictures in Fig. 4 present the results related to the driveline torsional oscillation attenuation and reduction of the longitudinal acceleration fluctuation described by variables ω_{sr} and a_x, respectively. To show the effectiveness of the proposed MPC micro-slip approach (blue line), we compare its performance considering a Proportional Integral (PI) micro-slip control architecture with direct compensation of the measured disturbances T_e and T_L (green line) and when the manoeuvre is performed without the micro-slip action (red line). The PI configuration can be intended as a baseline solution because of its simplicity and ease of design. The illustrations show a significant reduction of the oscillations in the considered manoeuvre for both ω_{sr} and a_x, as a result of activating the considered clutch micro-slip control strategies. We can quantify such an improvement by computing the RMS values ω_{sr}^{rms} and a_x^{rms} of the torsional speed and acceleration, respectively. We evaluate the RMS values by extracting the data from the release phases of the accelerator that occur at 2 and 7 s, which correspond to the light blue shaded areas. The results are summarized in Table 3 and show that the MPC approach improves the shuffle attenuation performance relative to PI and without micro-slip of about 9.8% and 20.6%, respectively. The

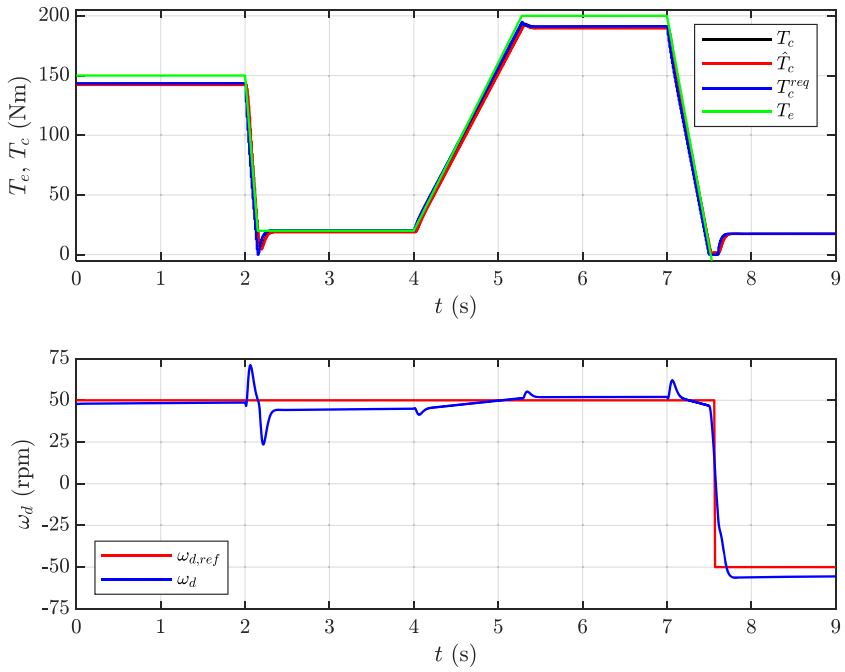

Fig. 3. Simulation Test for Nominal K_t. Top plot: Engine torque (green), requested clutch torque T_c^{req} (blue), actually transmitted clutch torque T_c (black) and estimated clutch torque $\widehat{T}_c$ (red). Bottom plot: Slipping speed reference ω_d^{ref} (red) and slipping speed ω_d (blue). (For interpretation of the references to colour in this figure legend, the reader is referred to the web version of this article.)

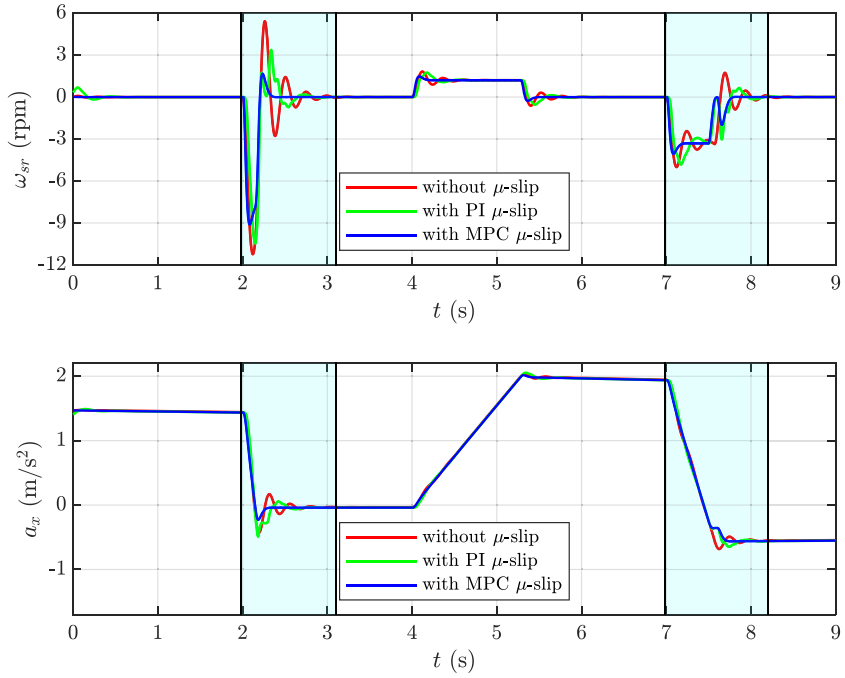

Fig. 4. Simulation Test: performance comparison with MPC micro-slip (blue), PI micro-slip (green) and without micro-slip (red). Top plot: Slipping speed ω_{sr}. Bottom plot: Longitudinal acceleration a_x. (For interpretation of the references to colour in this figure legend, the reader is referred to the web version of this article.)

Table 3
Simulation Test: performance comparison with and without micro-slip.

	MPC micro-slip	PI micro-slip	without micro-slip
ω_{sr}^{rms}	1.92	2.13	2.42
a_x^{rms}	0.50	0.54	0.56

improvement of longitudinal acceleration oscillation reduction of the MPC micro-slip is 7.4% and 10.7% relative to PI and without micro-slip, respectively.

To test the robustness properties of the designed MPC controller in the face of unaccounted uncertainty, two more simulations have been run in the presence of transmissibility coefficient K_t perturbations of $+$ 10% and $-$ 10% with respect to its nominal value. This means that, in such cases, the actuator provides an actual clutch torque T_c which is

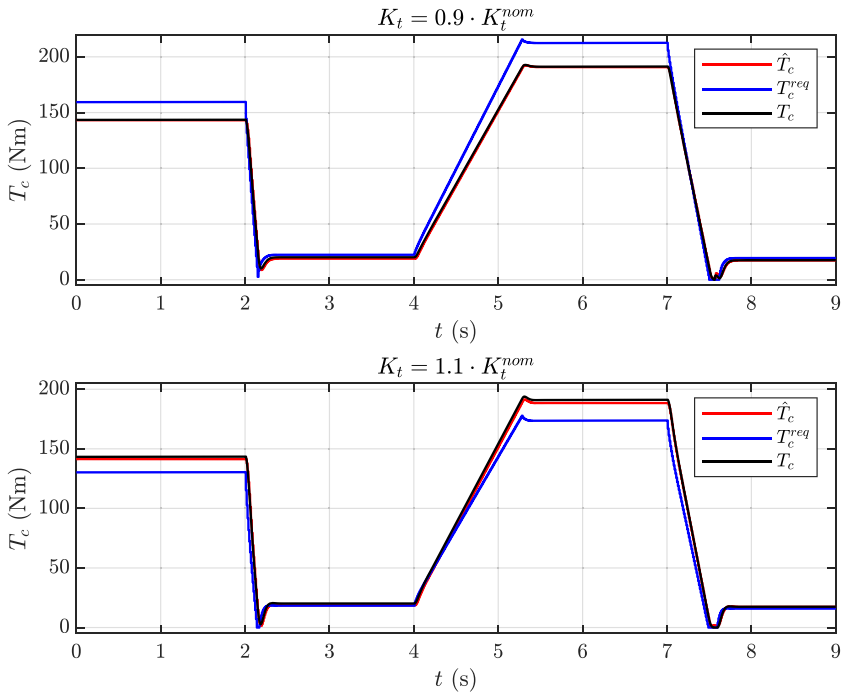

Fig. 5. Simulation Test with Perturbed K_t. Top plot -10% perturbation: Requested clutch torque T_c^{req} (blue), actually transmitted clutch torque T_c (black) and estimated clutch torque $\widehat{T}_c$ (red). Bottom plot $+10\%$ perturbation: Requested clutch torque T_c^{req} (blue), actually transmitted clutch torque T_c (black) and estimated clutch torque $\widehat{T}_c$ (red). (For interpretation of the references to colour in this figure legend, the reader is referred to the web version of this article.)

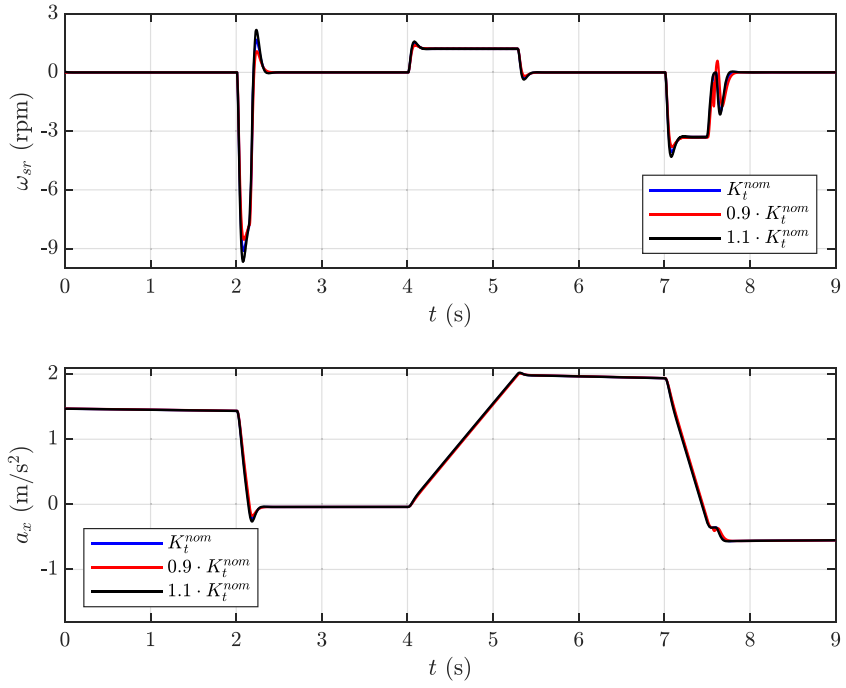

Fig. 6. Simulation Test with K_t Perturbed by $+10\%$ and -10%. Top plot: Slipping speed ω_{sr} comparison in the presence of nominal K_t (blue), $+10\%$ perturbed (black) and -10% perturbed (red). Bottom plot: Longitudinal acceleration a_x comparison in the presence of nominal K_t (blue), $+10\%$ perturbed (black) and -10% perturbed (red). (For interpretation of the references to colour in this figure legend, the reader is referred to the web version of this article.)

respectively larger or smaller than the corresponding requested one. In Fig. 5, the clutch torque plots obtained in such tests are reported. We notice that, in both plots of Fig. 5, the transmitted torque T_c courses (black lines) introduce approximately the same control action as in the case without transmissibility error shown in Fig. 3. Indicating that, even in the presence of perturbations on K_t, the MPC micro-slip control efficiently compensates such a transmissibility error by suitably regulating the torque request T_c^{req} to obtain the clutch action to achieve the required performance. As shown in top plot of Fig. 5, when the actual transmissibility is less than the nominal, a greater torque is requested by the controller. On the contrary, when K_t is greater than its nominal value, the MPC controller computes a lower requested torque, as can be

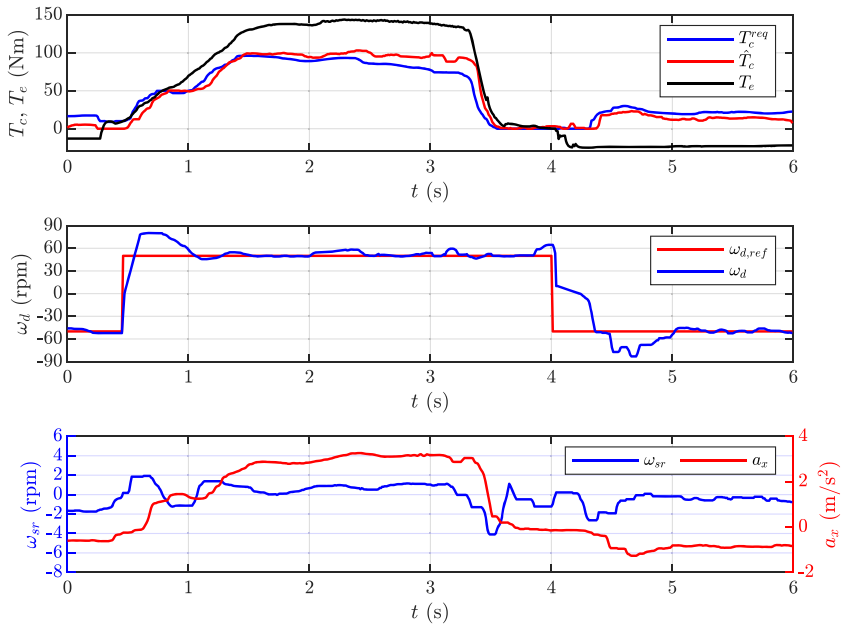

Fig. 7. Experimental Test: Tip-in and tip-out manoeuvre with micro-slip control, 1st gear. Top plot: Engine torque T_e (black), requested clutch torque T_c^{req} (blue) and estimated clutch torque $\widehat{T}_c$ (red). Middle plot: Slipping speed reference ω_d^{ref} (red) and slipping speed ω_d (blue). Bottom plot: Torsion speed ω_{sr} (blue) and longitudinal acceleration a_x (red). (For interpretation of the references to colour in this figure legend, the reader is referred to the web version of this article.)

seen in the bottom plot of Fig. 5.

The performance in terms of driveline oscillation attenuation obtained by the clutch micro-slip MPC control in the presence of transmissibility perturbation are reported in Fig. 6. The top picture of Fig. 6 shows the plots of ω_{sr}, to evaluate the results in terms of torsional oscillation attenuation. We notice that the effect of the transmissibility error is negligible with respect to case of nominal K_t. Only a slight degradation is observed for the case $0.9K_t^{nom}$ during the tip-out phase. A similar result is obtained for the jerking effect limitation, as shown in the bottom plot of Figure. 6. According to the results reported in Figs. 5 and 6, we can conclude that the proposed MPC approach to the clutch micro-slip control achieves quite good robustness properties in the presence of unaccounted transmissibility perturbation.

5. Experimental results

In this section, we introduce experimental results obtained on a prototype vehicle. We have realized the tests in manual driving operation, i.e., a human driver acts on the accelerator pedal to perform the requested manoeuvre. In such tests, the micro-slip MPC controller has

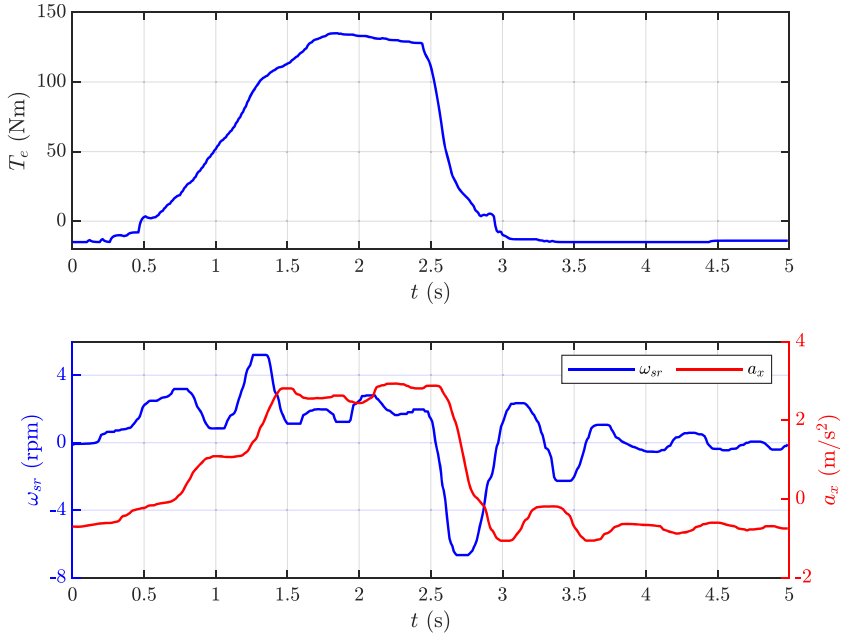

Fig. 8. Experimental Test: Tip-in tip-out manoeuvre without micro-slip, 1st gear. Top plot: Engine torque T_e. Bottom plot: Torsion speed ω_{sr} (blue) and Longitudinal acceleration a_x (red). (For interpretation of the references to colour in this figure legend, the reader is referred to the web version of this article.)

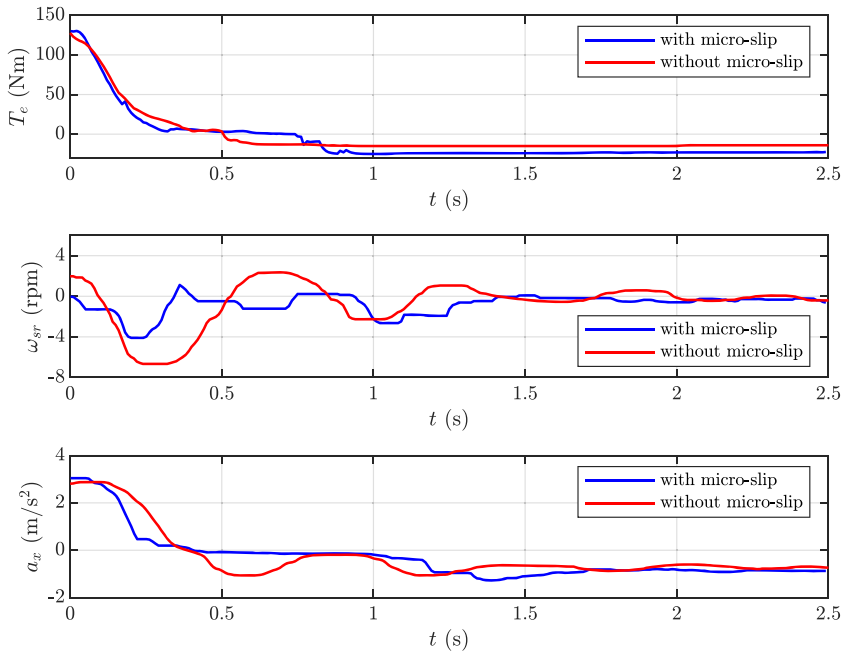

Fig. 9. Experimental Test: tip-out manoeuvre with (blue) and without (red) micro-slip, 1st gear. Top plot: Engine torque T_e. Middle plot: Torsion speed ω_{sr}. (For interpretation of the references to colour in this figure legend, the reader is referred to the web version of this article.)

been implemented on a commercial TCU characterized by a single precision floating point 32 bit processor working at a frequency of 100 MHz and equipped with a 1.5 MB embedded flash memory and a 64 kB on-chip static RAM, see Vafidis and Cimmino (2009) for details. The solution to the QP has been obtained through a fast active set algorithm similar to the one introduced in Ferreau et al. (2008) and employed in Canale and Casale-Brunet (2014). In this experimental setting, the prediction horizon is set to $N = 5$ and the mean computational time for a control move is about 1 ms, which satisfies the constraint given by the sampling time $T_s = 10$ ms. In order to optimize the vehicle performance, a slight retuning of the cost function weights was performed by means of a rapid prototyping environment like the one introduced in Canale et al. (2014).

5.1. Tip-in and tip-out test

In the tip-in manoeuvre, the driver suddenly pushes the gas pedal during a deceleration causing an increase of the engine torque request. On the contrary, during the tip-out manoeuvre, a sudden release of the gas pedal is issued when the vehicle is accelerating, providing an abrupt fall of the engine torque. In the experimental results introduced in this subsection, two tip-in and tip-out manoeuvre tests are performed when either the 1st or the 3rd gear is engaged.

In Fig. 7, we introduce the obtained results. In the upper plot of Fig. 7, we show the engine torque T_e enforced by the driver to realize the manoeuvre, the requested clutch torque T_c^{req}, reported in blue and the estimated transmitted torque $\widehat{T}_c$ plotted in red. We notice that there are differences between the estimated transmitted torque time profile and the requested one, which means that during this manoeuvre, transmissibility errors occurred. Despite the presence of such errors, the micro-slip control achieves good overall performance. In the middle plot of Fig. 7, the slipping speed ω_d is plotted (blue line) and compared with its reference signal ω_d^{ref} (red line), highlighting the quite good tracking performance. In the lower plot of Fig. 7, we report the torsion speed ω_{sr} and the longitudinal acceleration a_x, respectively. Both plots show smooth behaviours without oscillations during the gas pedal pressing and releasing phases.

To highlight the advantages of the micro-slip approach, a similar test was implemented in the absence of the micro-slip controller. During such a test, the clutch was kept closed, and the driveline directly transmitted the engine torque to the wheels. The results of this test are reported in Fig. 8 where, in the top plot, the engine torque T_e employed in the manoeuvre is shown while, in the lower plot, the resulting torsion speed ω_{sr} (blue) and longitudinal acceleration a_x (red) are shown. It is worth noting that during the tip-out phase significant oscillations on both ω_{sr} and a_x are induced by the accelerator action. Such oscillations occur for about 2 s in the absence of variations of the engine torque.

Table 4
Experimental tip-out manoeuvre, 1st gear: performance comparison with and without micro-slip.

	MPC micro-slip	without micro-slip
ω_{sr}^{rms}	1.24	2.27
a_x^{rms}	1.02	1.10

To better highlight the performance enhancement obtained by the MPC micro-slip controller, in Fig. 9, we compare the tip-out phase of the tests in terms of engine torque, torsional speed and longitudinal acceleration. As already done for the simulation results in Section 4, we quantify the improvements through the RMS values ω_{sr}^{rms} and a_x^{rms} of the torsional speed and acceleration, respectively, computed during this phase. Table 4 continues such a quantitative analysis showing that the MPC micro-slip improves the shuffle performance of about 45.3% and the longitudinal acceleration oscillation reduction of about 7.3%.

We also performed a tip-in tip-out experimental test when the 3rd gear is engaged. The engine torque T_e imposed by the driver is shown in the upper plot of Fig. 10, together with the requested clutch torque T_c^{req} and the estimated clutch torque $\widehat{T}_c$. In this manoeuvre, quite good performances are achieved in clutch torque estimation and slipping speed ω_d tracking; see the middle plot. The torsion speed ω_{sr} and the longitudinal acceleration a_x plots illustrated in the bottom part of Fig. 10 show a regular trajectory without significant oscillations.

The tip-in tip-out test with the 3rd gear engaged has been also performed without the micro-slip control. The results are reported in Fig. 11 where the plot of the imposed engine torque T_e, the obtained torsion speed ω_{sr} and longitudinal acceleration a_x are shown in the upper, and in

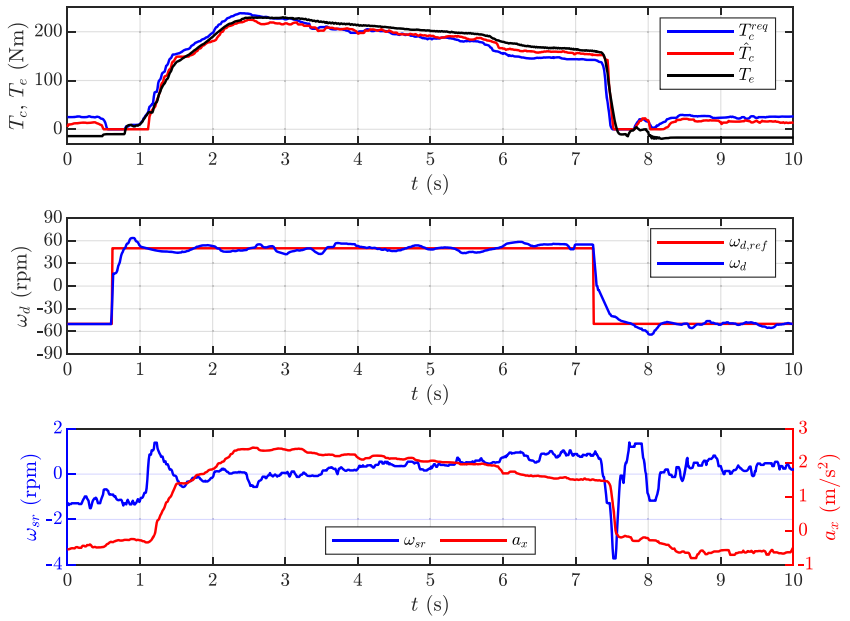

Fig. 10. Experimental Test: Tip-in and tip-out manoeuvre with micro-slip control, 3rd gear. Top plot: Engine torque T_e (black), requested clutch torque T_c^{req} (blue) and estimated clutch torque $\hat{T}_c$ (red). Middle plot: Slipping speed reference ω_d^{ref} (red) and slipping speed ω_d (blue). Bottom plot: Torsion speed ω_{sr} (blue) and longitudinal acceleration a_x (red). (For interpretation of the references to colour in this figure legend, the reader is referred to the web version of this article.)

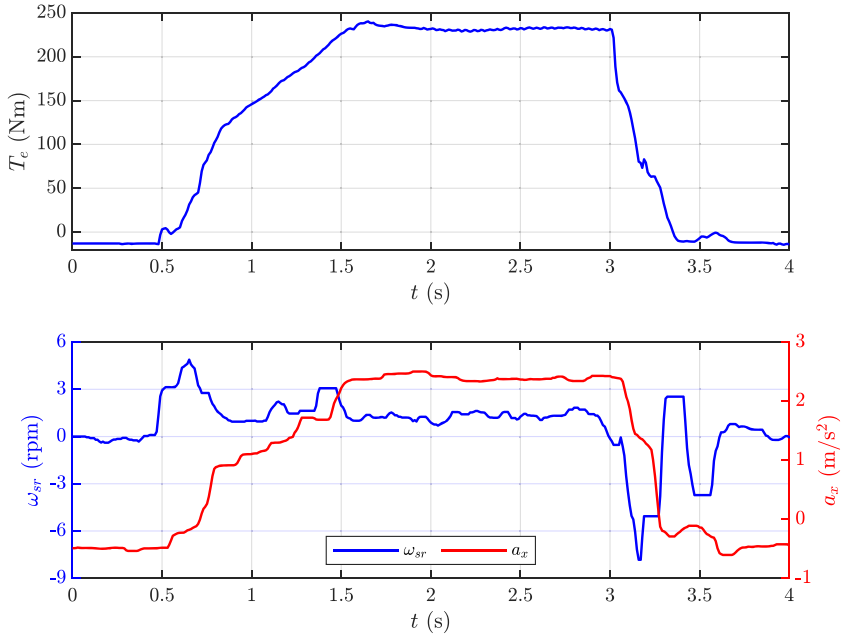

Fig. 11. Experimental Test: Tip-in tip-out manoeuvre without micro-slip, 3rd gear. Top plot: Engine torque T_e. Bottom plot: Torsion speed ω_{sr} (blue) and Longitudinal acceleration a_x (red). (For interpretation of the references to colour in this figure legend, the reader is referred to the web version of this article.)

the lower plots, respectively. It is worth noticing the oscillating behavior of the slipping speed and the acceleration in the final part of the manoeuvre when the engine torque is almost constant.

Fig. 12 shows a direct graphical comparison of the tip-out manoeuvre with and without micro-slip, highlighting the improvements introduced by the micro-slip for both the torsion speed and the longitudinal acceleration in terms of oscillation attenuation. Table 5 summarizes the quantitative results of the RMS values of ω_{sr} and a_x. We notice an enhancement of about 49.6% for the torsion speed and about 29.3% for the longitudinal acceleration.

5.2. Bump crossing test

This subsection introduces the experimental results obtained when the accelerator pedal release phase is followed by a bump crossing manoeuvre when the 1st gear is engaged. As for the tip-in tip-out test, we have performed two experiments, i.e., in the presence and the absence of the micro-slip control. In Fig. 13, we compare the profiles of the torsional speed and the longitudinal acceleration. The bump crossing occurs at time instant 0.32 s for micro-slip test and at time 0.42 s for the test without micro-slip. Such events are indicated with vertical dotted lines in Fig. 13. The plots in Fig. 13 highlight that the torsion speed ω_{sr}

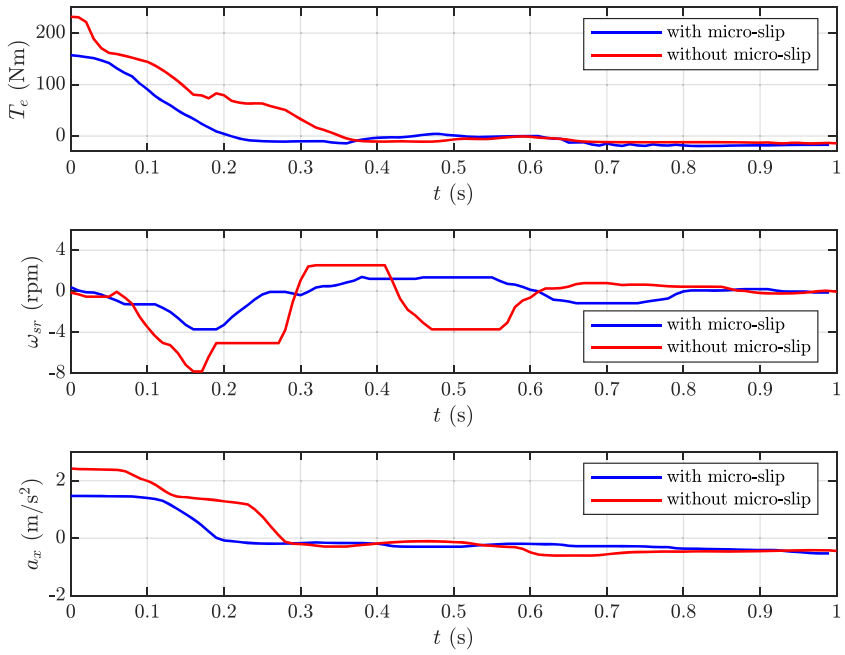

Fig. 12. Experimental Test: Tip-out manoeuvre with (blue) and without (red) micro-slip, 3rd gear. Top plot: Engine torque T_e. Middle plot: Torsion speed ω_{sr}. Bottom plot: Longitudinal acceleration a_x. (For interpretation of the references to colour in this figure legend, the reader is referred to the web version of this article.)

Table 5
Experimental tip-out manoeuvre, 3rd gear: performance comparison with and without micro-slip.

	MPC micro-slip	without micro-slip
ω_{sr}^{rms}	1.29	2.56
a_x^{rms}	0.65	0.92

Table 6
Experimental bump crossing manoeuvre: performance comparison with and without micro-slip.

	MPC micro-slip	without micro-slip
ω_{sr}^{rms}	0.95	2.89
a_x^{rms}	0.71	0.91

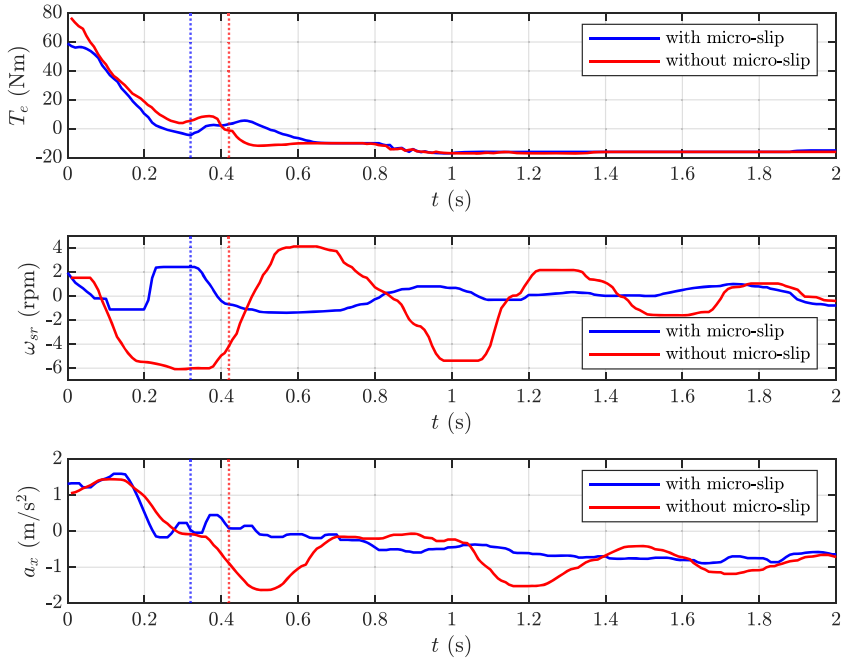

Fig. 13. Experimental Test: Bump crossing manoeuvre with (blue) and without (red) micro-slip control. Top plot: Engine torque T_e. Middle plot: torsion speed ω_{sr}. Bottom plot: longitudinal acceleration a_x. Bump crossing instants are highlighted with vertical dotted lines: blue with micro-slip and red without micro-slip. (For interpretation of the references to colour in this figure legend, the reader is referred to the web version of this article.)

and the acceleration a_x with micro-slip show relatively smooth trajectories. On the contrary, significant oscillation on ω_{sr} and a_x are evident in the manoeuvre performed without micro-slip. The RMS results reported in Table 6 quantify an enhancement of about 67.1% for ω_{sr} and about 21.9% for a_x.

6. Conclusion

In this work we have presented an original MPC approach to micro-slip clutch control for driveline torsional oscillation attenuation in vehicles with Automated Manual Transmission system. The proposed MPC formulation can effectively handle the performance tradeoff between the clutch slip regulation and the torsional oscillation attenuation. An observer is used to feedback the unmeasured states and obtain an estimate of the actual clutch torque. This allows us to cope with saturation constraints on the torque that is really transmitted by the actuator device. A piecewise-affine linear model with two switching modes describes the actuator-driveline dynamics to account for the case of special manoeuvres that cause an inversion in the transmission motion, like, e.g., tip-in and tip-out tests. Within such a context, a switching MPC approach is adopted where the underlying optimization problem is a quadratic programme for a fast online implementation of the controller on commercial transmission control unit platforms. Extensive simulations performed on a detailed driveline model and experimental vehicle tests show the effectiveness of the introduced approach.

Declaration of Competing Interest

The authors declare that they have no known competing financial interests or personal relationships that could have appeared to influence the work reported in this paper.

References

Albers, A. (1990). Torque control isolation (tci): the smart clutch. *4th luk symposium*.

Audi of America Inc. (2001). Variable automatic transmission multitronic 01j. *Self-study program course number 951103*.

Baumann, J., Torkzadeh, D. D., Ramstein, A., Kiencke, U., & Schlegl, T. (2006). Model-based predictive anti-jerk control. *Control Engineering Practice, 14*, 259–266.

Bemporad, A., Borrelli, F., Glielmo, L., & Vasca, F. (2001). Hybrid control of dry clutch engagement. *Proc. of European Control Conference*.

Berriri, M., Chevrel, P., & Lefebvre, D. (2008). Active damping of automotive powertrain oscillations by a partial torque compensator. *Control Engineering Practice, 16*, 874–883.

Borrelli, F., Bemporad, A., & Morari, M. (2017). *Predictive Control for Linear and Hybrid Systems*. Cambridge University Press.

Bruce, L., Egardt, B. S., & Pettersson, S. (2005). On powertrain oscillation damping using feedforward and lq feedback control. *IEEE Conference on Control Applications 2005* (pp. 1415–1420). IEEE.

Buerger, J., & Anderson, J. (2019). Robust control for electric vehicle powertrains. *Control Theory Technology, 17*(4), 382–392.

Canale, M., & Casale-Brunet, S. (2014). A multidisciplinary approach for model predictive control education: A lego mindstorms nxt-based framework. *International Journal of Control, Automation and Systems, 12*(5), 1030–1039.

Canale, M., Cerone, V., Baliva, S., & Corigliano, E. (2017). A model predictive control approach to micro-slip control of automated manual transmission systems. *American Control Conference (ACC), 2017* (pp. 3613–3618). IEEE.

Canale, M., Fagiano, L., Ruiz, F., & Signorile, M. (2008). A study on the use of virtual sensors in vehicle control. *47th IEEE Conference on Decision and Control* (pp. 4402–4407).

Canale, M., Razza, V., & Regruto, D. (2014). Model predictive control education using a rapid prototyping industrial platform. *International Journal of Engineering Education, 30*(6(A)), 1486–1498.

Caruntu, C. F., Lazar, M., & Cairano, S. D. (2016). Driveline oscillations damping: A tractable predictive control solution based on a piecewise affine model. *Nonlinear Analysis: Hybrid Systems, 19*, 168–185.

Caruntu, C. F., Lazar, M., Gielen, R. H., van den Bosch, P., & Cairano, D. (2013). Lyapunov based predictive control of vehicle drivetrains over can. *Control Engineering Practice, 21*, 1884–1898.

Corno, M., Dattilo, S., & Savaresi, S. (2021). Black-box model-based active damping of driveline oscillations. *European Control Conference (ECC), 2021* (pp. 921–926). EUCA.

Di Cairano, S., Tseng, E., Bernardini, D., & Bemporad, A. (2010). Steering vehicle control by switched model predictive control. *IFAC workshop advance in automotive control* (pp. 1–6). IFAC.

Dolcini, P., de Wit, C. C., & Béchart, H. (2005). Improved optimal control of dry clutch engagement. *16th IFAC World Congress, Prague, Czech Republic*. IFAC.

Ferreau, H., Bock, H., & Diehl, M. (2008). An online active set strategy to overcome the limitations of explicit mpc. *International Journal of Robust and Nonlinear Control, 18*(8), 816–830.

Fischer, R., & Berger, R. (1998). Automation of manual transmissions. *6th LUK Symposium*.

Fischer, R., Küçükay, F., Jürgens, G., Najork, R., & Pollak, B. (2015). *The Automotive Transmission Book*. Springer, Berlin.

Fredriksson, J., Weiefors, H., & Egardt, B. (2002). Powertrain control for active damping of driveline oscillations. *Vehicle System Dynamics, 37*(5), 359–376.

Gao, B. Z., Chen, H., Sanada, K., & Hu, Y. (2011). Design of clutch-slip controller for automatic transmission using backstepping. *IEEE/ASME Transactions on Mechatronics, 16*(3), 498–508.

Grüne, L., & Pannek, J. (2011). *Nonlinear Model Predictive Control: Theory and Algorithms*. Springer, London.

Heath, W. P., & Wills, A. G. (2005). The inherent robustness of constrained linear model predictive control. *16th IFAC World Congress* (pp. 71–76). IFAC.

Hebbale, K., Lee, C., Samie, F., Kao, C., Chen, X., Horgan, J., & Hearld, S. (2011). Model based torque converter clutch slip control. *SAE technical paper: 2011-01-0396*.

Higashimata, A., Adachi, K., Segawa, S., Kurogo, N., & Waki, H. (2004). Development of a slip control system for a lock-up clutch. *SAE technical paper: 2004-01-1227*.

Kaneko, Y., Adachi, K., Iino, F., & Hirata, M. (2009). Development of a slip control system for a lock-up clutch (part iii). *SAE technical paper: 2009-01-0955*.

Kiencke, U., & Nielsen, L. (2005). *Automotive control systems (2nd Edition)*. Springer, Berlin.

Lagerberg, A., & Egardt, B. (2005). Model predictive control of automotive powertrains with backlash. *16th IFAC World Congress, Prague, Czech Republic*. IFAC.

Lancia, E. (2014). *Modelling and parameter estimation of a DDCT transmission system*. MSc Dissertation, Politecnico di Torino.

Lee, D. (2015). Algorithm design for filtering input shaft speed from judder and minimize static error by phase advance methods. *SAE technical paper: 2015-01-0029*.

Lefebvre, D., Chevrel, P., & Richard, S. (2003). An h-infinity-based control design methodology dedicated to the active control of vehicle longitudinal oscillations. *IEEE Transactions on Control Systems Technology, 11*(6), 948–956.

Lhomme, W., Trigui, R., Delarue, P., Jeanneret, B., Bouscayrol, A., & Badin, F. (2008). Switched causal modeling of transmission with clutch in hybrid electric vehicles. *IEEE Transactions on Vehicular Technology, 57*(4), 2081–2089.

Lu, X., Chen, H., Gao, B., Zhang, Z., & Jin, W. (2015). Data-driven predictive gearshift control for dual-clutch transmissions and fpga implementation. *IEEE Transactions on Industrial Electronics, 62*(1), 599–610.

Mashadi, B., & Badrykoohi, M. (2015). Driveline oscillation control by using a dry clutch system. *Applied Mathematical Modelling*, 6471–6490.

Mayne, D. Q., Raković, S., Findeisen, R., & Allgöwer, F. (2006). Robust output feedback model predictive control of constrained linear systems. *Automatica, 42*(7), 1217–1222.

Mayne, D. Q., & Rawlings, J. B. (2012). *Model Predictive Control: Theory and Design*. Nob Hill Publishing.

Myklebust, A. (2014). *Dry Clutch Modeling, Estimation, and Control*. PhD Dissertation, Linköping University.

Naus, G. J. L., Beenakkers, M., Huisman, R., van de Molengraft, M. J. G., & Steinbuch, M. (2008). Robust control to suppress clutch judder. *8th International Symposium Advances Vehicle Control*.

Northcote, N. (2006). *The modeling and control of an automotive drivetrain*. MSc Dissertation, University of Stellenbosch.

Pettersson, M., & Nielsen, L. (2003). Diesel engine speed control with handling of driveline resonances. *Control Engineering Practice, 11*, 319–328.

Pisaturo, M., Cirrincione, M., & Senatore, A. (2015). Multiple constrained mpc design for automotive dry clutch engagement. *IEEE/ASME Transactions on Mechatronics, 20*(1), 469–480.

Ravichandran, M., Doering, J., Johri, R., & Ruybal, K. (2020). Design and evaluation of ev drivetrain clunk and shuffle management control system. *American Control Conference (ACC), 2020* (pp. 4905–4912). IEEE.

Reddy, P., Shahbakhti, M., Ravichandran, M., & Doering, J. (2023). Real-time predictive clunk control using a reference governor. *Control Engineering Practice, 135*, 105489.

Rostalski, P., Besselmann, T., Maric, M., Belsen, F. V., & Morari, M. (2007). A hybrid approach to modelling, control and state estimation of mechanical systems with backlash. *International Journal of Control, 80*(11), 1729–1740.

Templin, P., & Egardt, B. (2009). An lqr torque compensator for driveline oscillation damping. *IEEE Conference on Control Applications 2009* (pp. 352–356). IEEE.

Vafidis, C., & Cimmino, F. (2009). Fpt's high torque density dual clutch transmission (htd-ddct). *8th cti symposium "innovative automotive transmissions", berlin, germany*.

Wang, X., & Lu, T. (2022). Offline model predictive control approach to micro-slip control in gearshifts of dual clutch transmission. *Proc. IMechE Part K:Journal of Multi-body Dynamics, 236*(1), 84–98.